

# Spin-pairing correlations and spin polarization of Majorana bound states in two-dimensional topological-insulator systems

Kunhua Zhang, Junjie Zeng, Yafei Ren, and Zhenhua Qiao\*

*ICQD, Hefei National Laboratory for Physical Sciences at Microscale, and Synergetic Innovation Centre of Quantum Information and Quantum Physics, University of Science and Technology of China, Hefei, Anhui 230026, China and CAS Key Laboratory of Strongly-Coupled Quantum Matter Physics and Department of Physics, University of Science and Technology of China, Hefei, Anhui 230026, China*

(Received 24 December 2016; published 11 August 2017)

We demonstrate that a zero-energy Majorana bound state in a ferromagnetic insulator (FI)-superconductor (SC) junction formed on the edge of a two-dimensional topological insulator exhibits three types of spin-triplet pairing correlations, its spin-polarization direction is position independent in a ferromagnetic insulator, and demonstrates a spin-helix structure in a superconductor. These spin properties of Majorana bound states lead to anomalous selective equal-spin Andreev reflection. Similar behavior is found when the coupling between two Majorana bound states in a FI-SC-FI junction is invoked, though an additional weak spin-singlet pairing correlation is generated. These signatures can readily facilitate the experimental detection of spin-triplet correlations and spin polarization of Majorana bound states.

DOI: [10.1103/PhysRevB.96.085117](https://doi.org/10.1103/PhysRevB.96.085117)

## I. INTRODUCTION

Majorana fermions are exotic particles that are their own antiparticles [1], and have been suggested to exist as Majorana bound states (MBSs) in condensed matter systems [2]. Two spatially separated MBSs can define a qubit that stores information nonlocally and is robust against local sources of decoherence [3], which together with its non-Abelian statistics [4,5] make it exhibit potential applications in quantum information and quantum computation [6]. Several theoretical proposals were raised to realize such states, like topological insulators proximity-coupled with superconductors [7–10], semiconductor-superconductor heterostructures [11–14], and magnetic-atomic chains on superconductors [15]. Recently, intensive theoretical and experimental efforts have been made to verify the existence of MBSs in these systems by employing charge transport properties [16–30]. However, little attention has been paid to the spin-related phenomena of MBSs [31–34]. Furthermore, the in-depth classifications of spin-triplet correlations and spin polarization of MBSs are yet unclear, especially those in two-dimensional topological insulator systems [35–37]. And these characteristics are closely related to the resulting unusual spin-related transport, like the intriguing selective equal-spin Andreev reflection [31,33].

In this paper, we present a systematic study of spin-pairing correlations and spin polarization of MBS/MBSs in ferromagnetic insulator (FI)-superconductor (SC) and FI-SC-FI junctions formed at the boundary of a two-dimensional topological insulator. For the FI-SC junction, we find a zero-energy MBS, which possesses three types of spin-triplet pairing correlations and its spin-polarization orientation remains unchanged in the ferromagnetic insulator region. When two MBSs are coupled in the FI-SC-FI junction, an additional weak spin-singlet pairing correlation is generated. In both cases, the dominated spin-triplet correlations induce strongly contrasted widths of equal-spin Andreev reflection peaks for injected

electrons with different spin polarizations. As a consequence, the spin-pairing correlations and spin polarization of MBSs could be experimentally detected in spin-related transport measurements.

The rest of this paper is organized as follows. Section II describes the setup under study and gives the formalism. Sections III and IV present the results on the spin-pairing correlations and spin polarization of MBSs, the related transport properties, and discussions. Section V concludes this paper. Some auxiliary materials are given in Appendixes.

## II. MODEL AND FORMALISM

We consider two different one-dimensional setups, which are FI-SC and FI-SC-FI junctions formed at the boundary of a two-dimensional topological insulator as displayed in Figs. 1(a) and 1(b). The one-dimensional edge states proximity-coupled with a bulk ferromagnetic insulator and an *s*-wave superconductor [7] can be described by the following Bogoliubov-de Gennes equation in the representation spanned on the basis of  $\{\varphi_{\uparrow}, \varphi_{\downarrow}, \varphi_{\downarrow}^{\dagger}, -\varphi_{\uparrow}^{\dagger}\}$  [8,10]:

$$\begin{pmatrix} v_F \sigma_x p_x + \boldsymbol{\sigma} \cdot \mathbf{m} - \mu & \Delta e^{i\phi} \\ \Delta e^{-i\phi} & -v_F \sigma_x p_x + \boldsymbol{\sigma} \cdot \mathbf{m} + \mu \end{pmatrix} \psi = E \psi, \quad (1)$$

where  $\boldsymbol{\sigma} = (\sigma_x, \sigma_y, \sigma_z)$  and  $v_F$  are, respectively, Pauli matrices and the Fermi velocity of the topological-insulator edge states. The proximity effects are reflected by the magnetization  $\mathbf{m}$  and pair potential  $\Delta e^{i\phi}$  that occur only at the ferromagnetic insulator and superconductor regions separately. In Fig. 1(a), the magnetization  $\mathbf{m}$  is set to be  $(0, 0, m_L)$ , and in Fig. 1(b), it is set to be  $(0, 0, m_{L/R})$  at the left/right sides of the superconductor. In our calculations, the phase  $\phi$  of pair potential plays no role and thus is set to be zero below. The chemical potential  $\mu(x)$  is determined with respect to the Dirac point and is assumed to be independently tunable via gating or doping in each region [38].

\*qiao@ustc.edu.cn

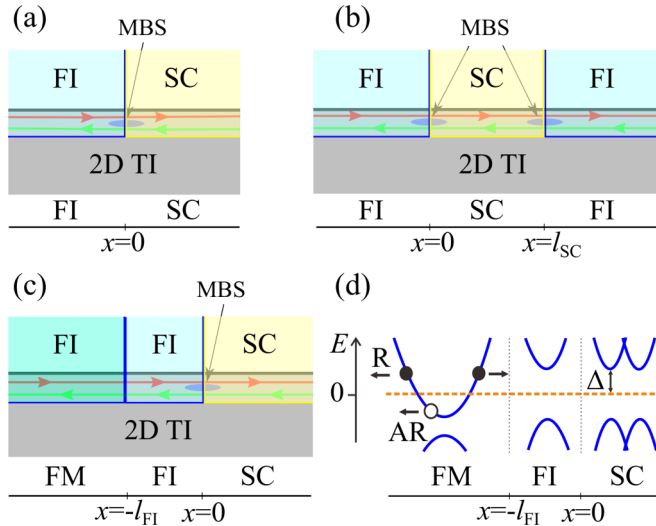


FIG. 1. (a)–(c) Schematics of one-dimensional FI-SC, FI-SC-FI, and ferromagnetic metal (FM)-FI-SC junctions mediated by the edge states of two-dimensional topological insulator (2D TI) systems, respectively. (d) Schematic energy band for the junction in (c). Solid and open circles indicate electrons and holes, respectively. R and AR indicate the electron reflection and Andreev reflection, respectively.

By solving Eq. (1), one can obtain the wave functions in the junctions shown in Fig. 1, e.g., the wave function in the left ferromagnetic insulator region of Fig. 1(a) is  $\psi_{\text{FI}}(x) = a_e(-\hbar v_{\text{F}} k_{\text{FI}}^+, E + \mu_{\text{FI}} - m_{\text{L}}, 0, 0)^T e^{-ik_{\text{FI}}^+ x} + a_h(0, 0, \hbar v_{\text{F}} k_{\text{FI}}^-, E - \mu_{\text{FI}} - m_{\text{L}})^T e^{-ik_{\text{FI}}^- x}$ , where  $k_{\text{FI}}^{\pm} = i\sqrt{m_{\text{L}}^2 - (\mu_{\text{FI}} \pm E)^2}/\hbar v_{\text{F}}$ ,  $\mu_{\text{FI}}$  is the chemical potential,  $a_{e/h}$  are the coefficients of evanescent wave functions for electron and hole, respectively. And the wave function in the right superconducting region is  $\psi_{\text{SC}}(x) = b(-e^{-i\alpha}, e^{-i\alpha}, -1, 1)^T e^{-ik_{\text{SC}} x - Kx} + c(e^{i\alpha}, e^{i\alpha}, 1, 1)^T e^{ik_{\text{SC}} x - Kx}$ , where  $k_{\text{SC}} = \mu_{\text{SC}}/\hbar v_{\text{F}}$ ,  $K = \Delta \sin \alpha/\hbar v_{\text{F}}$ , and  $\alpha = \arccos(E/\Delta)$  for  $E < \Delta$ . Here, the wave function is obtained under the condition that  $\mu_{\text{SC}}$  is much larger than  $\Delta$ .  $b$  and  $c$  are coefficients of the wave functions that are coherent superpositions of electron and hole excitations, and can be obtained by solving the continuity condition at the interface. In our consideration, chemical potentials and magnetizations in ferromagnetic insulators are, respectively, set to be zero and  $\Delta$ .

Spin-pairing correlations can be obtained from the retarded Green's function [35,36,39,40], which is closely related to the spectral function  $A(E, x) = \psi(x) \otimes \psi^\dagger(x)$  with  $\psi(x)$  being the wave function of the bound state [35]. The off-diagonal block  $A^{\text{off}}(E, x)$  can be expressed as

$$A^{\text{off}}(E, x) = \begin{pmatrix} 0 & d_0 \sigma_0 + \mathbf{d} \cdot \boldsymbol{\sigma} \\ d_0^* \sigma_0 + \mathbf{d}^* \cdot \boldsymbol{\sigma} & 0 \end{pmatrix}, \quad (2)$$

where  $\sigma_0$  is a  $2 \times 2$  identity matrix, and  $d_0$  and  $\mathbf{d}$  represent separately amplitudes of the spin-singlet and spin-triplet pairing correlations. To be specific,  $f_0 = d_0$  is the pairing amplitude of spin-singlet correlation  $|\uparrow\downarrow\rangle - |\downarrow\uparrow\rangle$ ;  $f_1 = -d_x + id_y$ ,  $f_2 = d_x + id_y$ , and  $f_3 = d_z$  are the pairing amplitudes of spin-triplet correlations  $|\uparrow\uparrow\rangle$ ,  $|\downarrow\downarrow\rangle$ , and  $|\uparrow\downarrow\rangle + |\downarrow\uparrow\rangle$ , respectively.

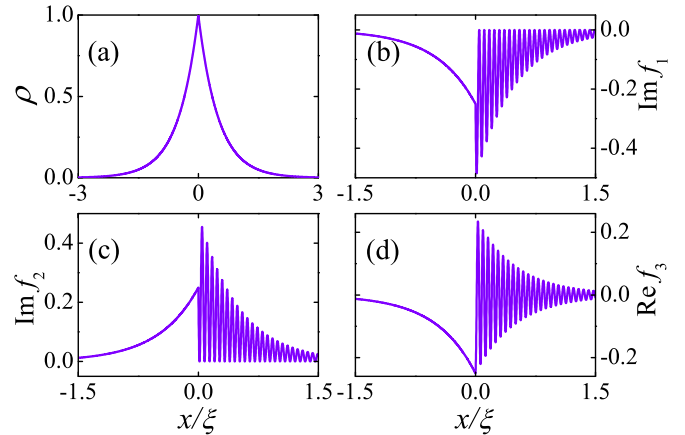


FIG. 2. (a) Probability density  $\rho$  of the zero-energy MBS as a function of  $x$ , with  $x = 0$  the interface of FI-SC junction. (b)–(d) Plot of spin-triplet pairing correlations  $|\uparrow\uparrow\rangle$ ,  $|\downarrow\downarrow\rangle$ , and  $|\uparrow\downarrow\rangle + |\downarrow\uparrow\rangle$  in FI-SC junction, respectively. Here, the chemical potential is  $\mu_{\text{SC}} = 50\Delta$ , and the superconducting coherence length is defined as  $\xi = \hbar v_{\text{F}}/\Delta$ .

### III. SINGLE MAJORANA BOUND STATE

In an FI-SC junction as displayed in Fig. 1(a), a zero-energy MBS can be formed on the boundary of a two-dimensional topological insulator where the gapless edge modes can be driven to open up a band gap by either ferromagnetism or an  $s$ -wave superconducting pair potential due to its spin-momentum locking. The probability density  $\rho(x) = \psi^\dagger(x)\psi(x)$  of this bound state is plotted in Fig. 2(a) as a function of position  $x$  where one can find that  $\rho$  decays exponentially with the increase of  $|x|$  indicating that the MBS is localized around the interface. We further calculate the spectral function and find a vanishing value of  $d_0$ . Thus there is no spin-singlet pairing correlation. However, spin-triplet pairing correlations are present since  $\mathbf{d}$  is not zero, whose component  $d_x$  is a pure imaginary number while  $d_{y,z}$  are real numbers, which are clearly given in Appendix A. Therefore the spin-triplet pairing correlation amplitudes  $f_{1,2} = \mp d_x + id_y$  have only imaginary parts, while  $f_3 = d_z$  has only a real part as plotted in Figs. 2(b)–2(d), where these amplitudes are also localized around the interface and exhibit the Friedel-type spatial oscillation in the  $x > 0$  superconducting region with a periodicity of  $1/k_{\text{SC}}$ .

The existence of spin-triplet pairing correlation indicates that the MBS could have nonzero spin polarization  $s_i(x) = \psi^\dagger(x)(\tau_z \otimes \sigma_i)\psi(x)$ , where  $i = x, y, z$  and  $\tau_z$  describes the particle-hole degree of freedom [34,41]. We find that the  $x$ -component  $s(x)$  of spin polarization vanishes in the whole region while the  $z$  component is also zero in the ferromagnetic insulator region as shown in Fig. 3(a), where the spin polarization is plotted as a function of position  $x$ . It shows that in the superconductor region of  $x > 0$ , the local spin polarization of the MBS varies dramatically and exhibits a spin helix structure; while in the ferromagnetic insulator region (i.e.,  $x < 0$ ), the spin polarization orients along  $-y$  direction, perpendicular to the magnetization  $\mathbf{m}$  of the ferromagnetic insulator. We notice that, to our surprise, the local spin-polarization direction of MBS is the same as that of the Cooper pair near the interface, which can be obtained by  $s_{\text{C}}(x) = i(\mathbf{d} \times \mathbf{d}^*)/|\mathbf{d}|^2$ ,

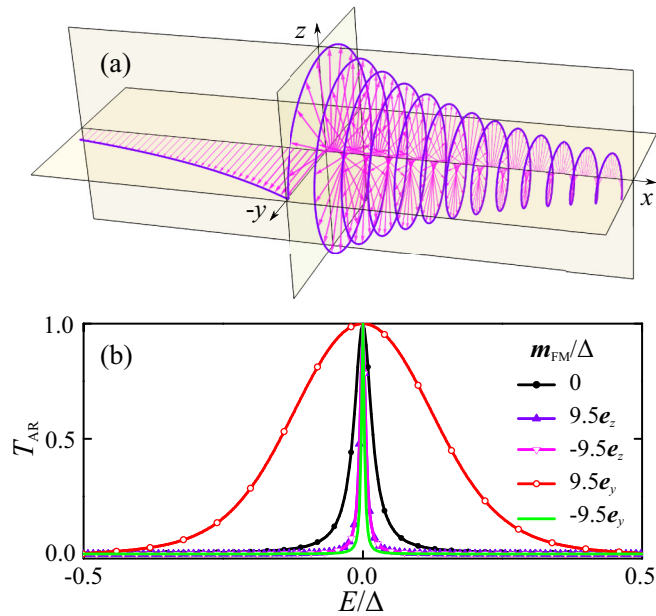


FIG. 3. (a) Local spin polarization of the MBS  $s(x)$  changes as a function of position  $x \in [-0.7\xi, 0.8\xi]$ , which is in the  $y$ - $z$  plane. (b) Probability of Andreev reflection  $T_{AR}$  as a function of excitation energy  $E$  of the incident electron for different magnetization  $\mathbf{m}_{FM}$ . Here, we choose  $l_{FI} = 2\xi$ ,  $\mu_{FM} = 10\Delta$ , and  $\mu_{SC} = 50\Delta$ .

where subscript  $C$  is employed to distinguish this quantity from the spin polarization of MBS  $s(x)$  [42].

After understanding the spin-pairing correlations and spin polarization of the MBS, one can naturally determine the spin-related transport property. For example, the spin-triplet pairing correlations can result in a selective equal-spin Andreev reflection, and the orientation of spin polarization of MBS further dominates the selective direction. Therefore spin-related properties of MBS in FI-SC can be experimentally detected by using the transport setup displayed in Fig. 1(c), where a ferromagnetic metal (FM) lead is connected to the FI-SC junction. The ferromagnetic metal is formed on the edge of a two-dimensional topological insulator where the ferromagnetism can be induced by the proximity effect of a ferromagnetic insulator and the metallic state can be induced by tuning the Fermi energy as indicated in Fig. 1(d). Moreover, the magnetization of the ferromagnetic metal is controllable and can be changed to any direction  $\mathbf{m}_{FM} = (m_x, m_y, m_z)$ . In order to utilize the electronic transport property in the junction, the length of the ferromagnetic insulator should be carefully chosen. In our consideration, we set  $l_{FI} = 2\xi$ . Figure 3(b) displays the probability of Andreev reflection  $T_{AR}$  as a function of excitation energy  $E$  for different  $\mathbf{m}_{FM}$ , the calculation of which is given in Appendix B. One can see that the zero-energy MBS leads to resonant Andreev reflection at  $E = 0$ , and the Andreev reflection peak has a finite width, which measures the coupling strength between the lead and the superconductor through the ferromagnetic insulator [cf. Fig. 1(d)].

It is noteworthy that the coupling strength between the lead and the superconductor depends obviously on the magnetization  $\mathbf{m}_{FM}$  in the ferromagnetic metal lead and the spin polarization of MBS in the middle ferromagnetic insulator,

which could lead to spin-flip scattering in the ferromagnetic insulator for the incident electron as described below. In the lead, the spin of an incident electron is parallel to  $(\hbar v_F k^+ + m_x, m_y, m_z)^T$ , while that of an Andreev reflected hole is parallel to  $(-\hbar v_F k^- + m_x, m_y, m_z)^T$ , where  $k^\pm = \sqrt{(\mu_{FM} \pm E)^2 - m_z^2 - m_y^2 \mp m_x} / \hbar v_F$ . For vanishing  $\mathbf{m}_{FM}$ , the spins of incident electron and reflected hole in the lead are respectively along  $+x$  and  $-x$  axes, but in the ferromagnetic insulator, these spins are flipped to  $y$  axis to match the spin polarization of MBS. Due to the spin-flip scattering, the Andreev reflection exhibits a narrow peak as displayed by the black solid-circled line in Fig. 3(b). For a very large  $\mathbf{m}_{FM}$  pointing along  $+y$  axis, the spins of incident electron and reflected hole in the lead are both approximately along  $+y$  axis, equal spin Andreev reflection occurs for the weakest spin-flip scattering, and the Andreev reflection peak exhibits the widest width as displayed by the red empty-circled line in Fig. 3(b). As a comparison, for large  $\mathbf{m}_{FM}$  pointing along  $-y$  axis, the strongest spin-flip scattering occurs in the ferromagnetic insulator, leading to the narrowest peak of the equal-spin Andreev reflection as displayed by the green line in Fig. 3(b). And a clearer dependence of Andreev reflection on the direction of  $\mathbf{m}_{FM}$  in the lead is given through the dependence of the peak width of Andreev reflection at half-height on the direction of  $\mathbf{m}_{FM}$  in Fig. 7 in Appendix B. These remarkable transport signatures can be utilized to verify the presence of spin-triplet correlations and determine the spin polarization of MBS.

The above phenomenon of equal-spin Andreev reflection in our system is anomalous compared with that induced by the MBS in the vortex core of a topological superconductor or semiconductor-superconductor heterostructures, where the equal-spin Andreev reflection peak has the widest width when the spin orientation of incident electrons is parallel to that of MBS [31,33,43], because in FI-SC junctions the spin polarization of MBS in a ferromagnetic insulator region is determined by the evanescent wave function in  $-x$  direction as given in above, while in FM-FI-SC junctions, the wave function of incident electrons in a ferromagnetic metal lead moving along  $x$  direction is matched with the evanescent wave function moving in  $x$  direction in a ferromagnetic insulator, which is  $\psi'_{FI}(x) = n_e(\hbar v_F k_{FI}^+, E + \mu_{FI} - m_L, 0, 0)^T e^{ik_{FI}^+ x} + n_h(0, 0, -\hbar v_F k_{FI}^-, E - \mu_{FI} - m_L)^T e^{ik_{FI}^- x}$ . Such evanescent wave function has opposite spin polarization compared to that of the MBS wave function, also in fact, the MBS wave function is the reflected wave function of  $\psi'_{FI}(x)$  in a FM-FI-SC junction. Based on the above transport phenomenon, it can be concluded that the spin properties of MBSs lead to selective equal-spin Andreev reflection, in which an electron with the opposite spin of MBSs will be reflected as a hole with the same spin as the incident electron and an electron with the same spin of MBSs will be reflected as an electron with unchanged spin. So this selective equal-spin Andreev reflection is anomalous compared with that found before.

#### IV. TWO COUPLED MAJORANA BOUND STATES

Now, we move to the system with coupling between two MBSs at the two interfaces of a superconductor in an

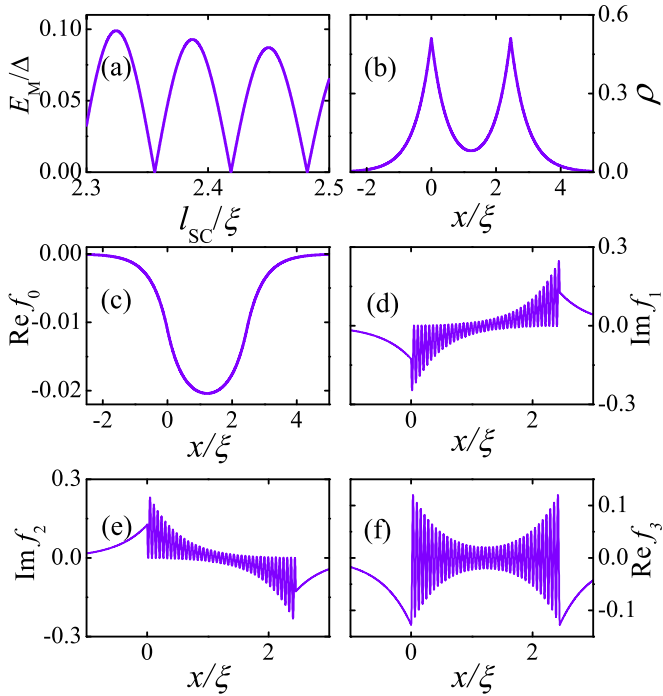


FIG. 4. (a) Coupling energy  $E_M$  of two MBSs as a function  $l_{SC}$ . (b) Probability density of the fermionic state formed by two coupled MBSs as a function of  $x$ , with  $x = 0, 2.45\xi$  being the two interfaces of FI-SC-FI junction. (c)–(f) Amplitudes of spin-pairing correlations  $|\uparrow\downarrow\rangle - |\downarrow\uparrow\rangle$ ,  $|\uparrow\uparrow\rangle$ ,  $|\downarrow\downarrow\rangle$ , and  $|\uparrow\downarrow\rangle + |\downarrow\uparrow\rangle$ , respectively. Here,  $\mu_{SC} = 50\Delta$ .

FI-SC-FI junction as displayed in Fig. 1(b). When the length of the superconductor  $l_S$  is finite, the wave functions of two MBSs overlap and are coupled to each other with a coupling energy of  $E_M$ , which splits the two zero-energy MBSs into two fermionic states of energies  $\pm E_M$ . As displayed in Fig. 4(a),  $E_M$  decreases and oscillates with the increase of the length of superconductor  $l_{SC}$  [17,44]. Such oscillation can be approximated as  $E_M e^{-l_{SC}/\xi} \cos(\mu_{SC} l_{SC}/\hbar v_F)$ , which implies that the coupling energy also oscillates with increasing  $\mu_{SC}$ . We further plot the probability density  $\rho(x)$  for the fermionic state of  $E_M$  in Fig. 4(b) as a function of  $x$ , where one can clearly see that  $\rho$  reaches the maxima at two interfaces indicating the nonlocality of the wave function. This character also manifests itself for the fermionic state of  $-E_M$ .

Different from the single MBS, these two fermionic states possess a weak spin-singlet pairing correlation as shown in Fig. 4(c), which takes the maximum at the center of the superconductor and is much smaller than the spin-triplet ones shown in Figs. 4(d)–4(f), where  $f_{1,2}$  are also pure imaginary while  $f_3$  is real. From these figures, one can find that the spin-triplet pairing correlations are maximized around both  $x = 0$  and  $l_{SC}$  and oscillate spatially in the superconductor, partly showing the characteristics of two decoupled MBSs. We further explore the local spin polarizations  $s(x)$  of the fermionic states, and find that they also have only finite  $y$ -component  $s_y$  in the two ferromagnetic insulator regions and have no  $x$ -component  $s_x$  in the superconductor region. Figure 5(a) displays the spin polarization of coupled MBSs as a function of  $x$ . It shows that the local spin polarization

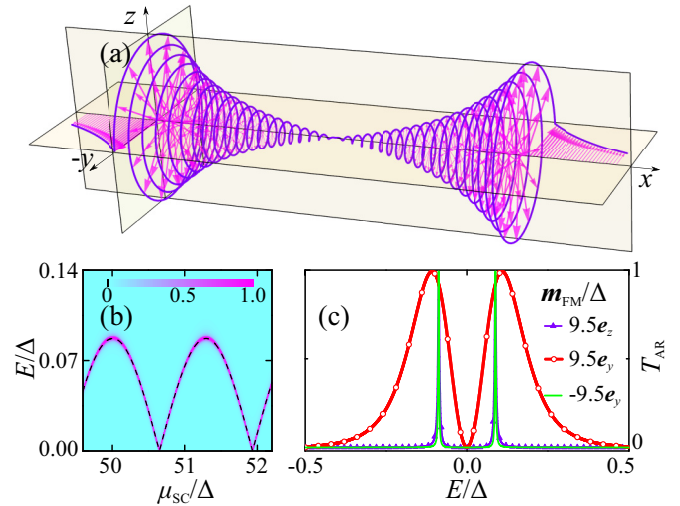


FIG. 5. (a) Local spin polarization of the fermionic state formed by two coupled MBSs  $s(x)$  as a function of position  $x \in [-0.5\xi, 3\xi]$ , with  $\mu_{SC} = 50\Delta$ . (b) Probability of Andreev reflection  $T_{AR}$  as a function of excitation energy  $E$  of the incident electron and  $\mu_{SC}$ , with the black-dashed line being the coupling energy of the two MBSs. (c)  $T_{AR}$  as a function of  $E$  for different magnetizations  $m_{FM}$  with  $\mu_{SC} = 50\Delta$ . In (b) and (c),  $l_{FI} = 2\xi$  and  $\mu_{FM} = 10\Delta$ .

direction changes spatially manifesting itself as a spin helix in the superconductor region, while is fixed along  $\mp y$  direction in the left and right ferromagnetic insulator and is perpendicular to the magnetization  $\mathbf{m}$  in both ferromagnetic insulators. Due to the nonuniform magnetization and superconducting potential in ferromagnetic insulator-superconductor-ferromagnetic insulator heterojunctions, the magnetizations in two ferromagnetic insulators can be different and well controlled, so the spin-polarization direction can be well manipulated to change in space as is shown in Appendix C.

In contrast to the single MBS, the Andreev reflection probability  $T_{AR}$  shows strong tunability by changing the chemical potential of the superconductor,  $\mu_{SC}$ . In Fig. 5(b), we plot  $T_{AR}$  as a function of  $\mu_{SC}$  and energy  $E$  of the incident electron, where we find that, given  $\mu_{SC}$ , the resonant peak occurs when  $E$  is close enough to  $\pm E_M$  as indicated by the black dashed line. Therefore the energy spacing of these two peaks of  $T_{AR}$  corresponds is twice the coupling energy  $2E_M$ . By changing  $\mu_{SC}$ , one can find that the energy spacing of these two resonance peaks oscillates as shown in Fig. 5(b), which is in agreement with the dependence of  $E_M$  on  $\mu_{SC}$ . This dependence of  $T_{AR}$  on  $\mu_{SC}$  provides unambiguous evidence for the existence of MBSs by the measurement of charge conductance. Moreover, the width of the resonance peak is also spin-orientation dependent as shown in Fig. 5(c), which displays the probability of Andreev reflection  $T_{AR}$  in the FM-FI-SC-FI junction. It is found that when  $m_{FM}$  is positively large along the  $y$  direction,  $T_{AR}$  provides the widest peak as shown by the red dotted line; while when  $m_{FM}$  is negatively large along the  $-y$  direction,  $T_{AR}$  gives the narrowest peak as shown by the green curve. The dependence of  $T_{AR}$  on the magnetization of the ferromagnetic metal lead originates from the same physics as that for the FM-FI-SC junction. Therefore the splitting of  $T_{AR}$  peak and its dependence on

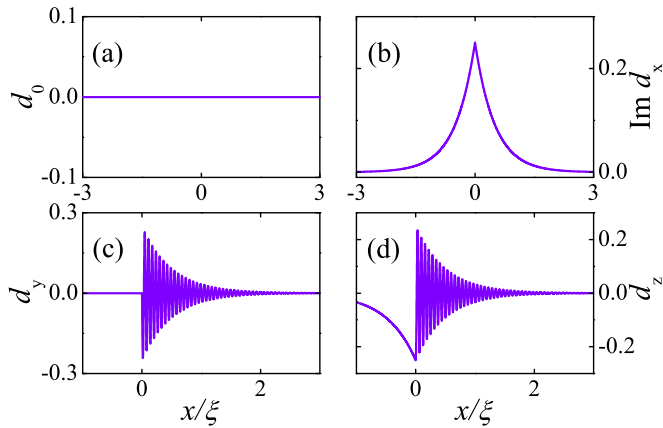


FIG. 6. Vector  $\mathbf{d}$  of zero Majorana bound state, (a)–(d) for the  $d_0$  of spin-singlet pairing, and vector  $d_x$ ,  $d_y$ , and  $d_z$  of spin-triplet pairing, respectively. Parameters are the same as in Fig. 2 in the main text.

the magnetization can be utilized to detect the spin-triplet correlations and spin polarization of coupled MBSs, e.g., by directly measuring the differential conductance in experiment.

## V. CONCLUSIONS

In summary, we show that a single zero-energy MBS at the boundary of a two-dimensional topological insulator exhibits three types of spin-triplet pairing correlations, while for two coupled MBSs there exists an additional weak spin-singlet pairing correlation. The dominated spin-triplet pairing correlations lead to nonzero spin-polarization of MBSs, which has a spin-helix structure in the superconducting region, while remains in the same direction in every ferromagnetic insulator region. By constructing a transport setup, it is found that the Andreev reflection peak has the widest (narrowest) width when an incident electron has a spin-polarization (anti-)parallel to that of MBS in ferromagnetic insulator. So it can be concluded that the spin properties of MBSs lead to anomalous selective equal-spin Andreev reflection in our system.

## ACKNOWLEDGMENTS

This work was financially supported by the National Key R & D Program (2016YFA0301700), NNSFC (11474265), the China Government Youth 1000-Plan Talent Program, Fundamental Research Funds for the Central Universities (WK3510000001 and WK2030020027), and China Postdoctoral Science Foundation (Grant No. 2016M590569). The Supercomputing Center of USTC is gratefully acknowledged for the high-performance computing assistance. K. Z. acknowledges Xin Liu and Qiang Cheng for helpful discussions.

## APPENDIX A: AMPLITUDES OF SPIN-SINGLET AND -TRIPLET VECTOR $d$ OF ZERO MAJORANA BOUND STATE

Here, we plot the amplitudes of spin singlet  $d_0$  and the vector of spin triplet  $\mathbf{d} = (d_x, d_y, d_z)$  of a single zero-energy Majorana bound state in Fig. 6. It can be found that there is

no spin-singlet pairing correlation, and spin-triplet pairing  $d_x$  is purely imaginary, while  $d_y$  and  $d_z$  are real numbers. The components of  $\mathbf{d}$  vector are asymmetric in the position space around interface  $x = 0$ . All the information about the spin-pairing correlation and spin polarization can be obtained by studying them. We also can get the amplitudes of spin singlet and the vector of spin triplet of the coupled Majorana bound state, the spin-triplet vector of which has similar characteristics as that of zero Majorana bound states, but the spin singlet of which has nonzero amplitude (not shown here).

## APPENDIX B: CALCULATION FOR THE ANDREEV REFLECTION

We give the calculation method for the Andreev reflection in the ferromagnet-ferromagnetic insulator-superconductor (FM-FI-SC) junction in Fig. 1(c) in the main text. Solving Eq. (1) in the main text, we obtain the wave function in the left FM region as  $\psi_{\text{FM}}(x) = (\hbar v_{\text{F}} k_{\text{FM}} + m_{\text{FMz}} - im_{\text{FMy}}, \varepsilon + \mu_{\text{FM}} - m_{\text{FMz}}, 0, 0)^T e^{ik_{\text{FM}}x} + r_{\text{e}}(-\hbar v_{\text{F}} k_{\text{FM}} - im_{\text{FMy}}, \varepsilon + \mu_{\text{FM}} - m_{\text{FMz}}, 0, 0)^T e^{-i(k_{\text{FM}} + \frac{2m_{\text{FMz}}}{\hbar v_{\text{F}}})x} + r_{\text{h}}(0, 0, -\hbar v_{\text{F}} k'_{\text{FM}} + m_{\text{FMz}} - im_{\text{FMy}}, \varepsilon - \mu_{\text{FM}} - m_{\text{FMz}})^T e^{ik'_{\text{FM}}x}$ , where the chemical potential  $\mu_{\text{FM}}$  is taken to lie in the conduction bands of the electronic states and  $\mu_{\text{FM}} > 0$ . Then  $k_{\text{FM}} = (\sqrt{(\varepsilon + \mu_{\text{FM}})^2 - m_{\text{FMz}}^2 - m_{\text{FMz}}^2} - m_{\text{FMz}})/\hbar v_{\text{F}}$  and  $k'_{\text{FM}} = (\sqrt{(\varepsilon - \mu_{\text{FM}})^2 - m_{\text{FMz}}^2 - m_{\text{FMz}}^2} + m_{\text{FMz}})/\hbar v_{\text{F}}$ .  $r_{\text{e}}$  and  $r_{\text{h}}$  are the coefficients of wave functions for normal reflection and local Andreev reflection, respectively. Note that the  $T$  in the wave functions indicates the transpose in this paper. The wave function in the FI region is  $\psi_{\text{FI}}(x) = a(\hbar v_{\text{F}} k_{\text{FI}}, \varepsilon + \mu_{\text{FI}} - m_{\text{FIz}}, 0, 0)^T e^{ik_{\text{FI}}x} + a'(-\hbar v_{\text{F}} k_{\text{FI}}, \varepsilon + \mu_{\text{FI}} - m_{\text{FIz}}, 0, 0)^T e^{-ik_{\text{FI}}x} + b(0, 0, -\hbar v_{\text{F}} k'_{\text{FI}}, \varepsilon - \mu_{\text{FI}} - m_{\text{FIz}})^T e^{ik'_{\text{FI}}x} + b'(0, 0, \hbar v_{\text{F}} k'_{\text{FI}}, \varepsilon - \mu_{\text{FI}} - m_{\text{FIz}})^T e^{-ik'_{\text{FI}}x}$ , where  $k_{\text{FI}} = i\sqrt{-(\mu_{\text{FI}} + \varepsilon)^2 + m_{\text{FIz}}^2}/\hbar v_{\text{F}}$ , and  $k'_{\text{FI}} = i\sqrt{-(\mu_{\text{FI}} - \varepsilon)^2 + m_{\text{FIz}}^2}/\hbar v_{\text{F}}$ . And the wave function in SC region is  $\psi_{\text{SC}}(x) = c(-e^{-i\alpha}, e^{-i\alpha}, -1, 1)^T e^{-ik_{\text{SC}}x - Kx} + d(e^{i\alpha}, e^{i\alpha}, 1, 1)^T e^{ik_{\text{SC}}x - Kx}$ , where  $k_{\text{SC}} = \mu_{\text{SC}}/\hbar v_{\text{F}}$ ,  $K = \frac{\Delta \sin \alpha}{\hbar v_{\text{F}}}$ ,  $\alpha = \arccos(\varepsilon/\Delta)$  for  $\varepsilon < \Delta$ .  $c$  and  $d$  are coefficients of the wave functions, which are coherent superpositions of electron and hole excitations.

The wave functions in different regions are matched by the boundary conditions,  $\psi_{\text{FM}}(x = -l_{\text{FI}}) = \psi_{\text{FI}}(x = -l_{\text{FI}})$  and  $\psi_{\text{FI}}(x = 0) = \psi_{\text{SC}}(x = 0)$ , which give the probabilities of all the transport processes through this following matrix:

$$\begin{pmatrix} 1 \\ r_{\text{e}} \\ r_{\text{h}} \\ 0 \end{pmatrix} = M \begin{pmatrix} c \\ 0 \\ d \end{pmatrix}, \quad (\text{B1})$$

where  $M$  is a  $4 \times 4$  matrix, whose matrix elements are determined by the boundary conditions of wave functions. And the probability of Andreev reflection is  $r_{\text{h}}^* r_{\text{h}} \frac{(\varepsilon - \mu_{\text{FM}} - m_{\text{FMz}})(\hbar v_{\text{F}} k'_{\text{FM}} - m_{\text{FMz}})}{(\varepsilon + \mu_{\text{FM}} - m_{\text{FMz}})(\hbar v_{\text{F}} k_{\text{FM}} + m_{\text{FMz}})}$ , which can be used for calculating the probability of Andreev reflection  $T_{\text{AR}}$  in Fig. 3(b) in the main text. The same way as above can be used to calculate  $T_{\text{AR}}$  in Figs. 5(b) and 5(c) for the FM-FI-SC-FI junction in the main text.

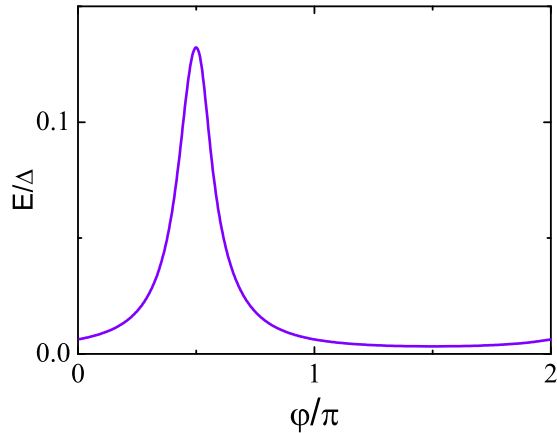


FIG. 7. The energy  $E$  of incident electron as a function of azimuthal angle  $\varphi$  in the  $y$ - $z$  plane at the half-height of each peak of the probability of Andreev reflection  $T_{AR}$ . Parameters are the same as in Fig. 3(b) in the main text.

In addition, we plot the energy  $E$  of incident electrons as a function of azimuthal angle  $\varphi$  ( $\sin \varphi = m_z/m$ ,  $\cos \varphi = m_y/m$ ,  $m = |\mathbf{m}_{FM}|$ ) in the  $y$ - $z$  plane in Fig. 7, under the condition that the peak width of Andreev reflection is at half height. It can be found that the dependence of  $E$  on  $\varphi$  is quite anisotropic, which gives a more clear description for Fig. 3(b) in the main text about its dependence on the direction of the magnetization in the ferromagnetic lead.

### APPENDIX C: SPIN POLARIZATION OF COUPLED MAJORANA BOUND STATES

We plot the spin polarization of coupled Majorana bound states as a function of position  $x$  in Fig. 8. It can be found that

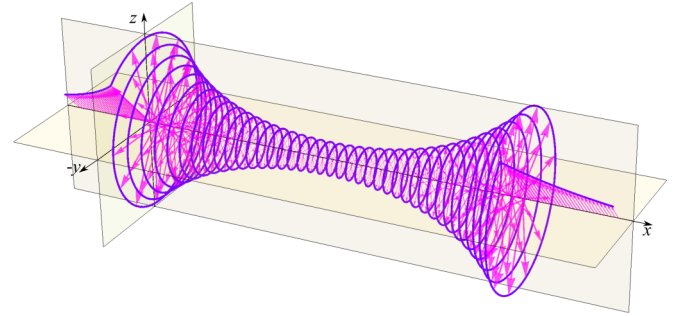


FIG. 8. Local spin polarization of the fermionic state formed by two coupled MBSs  $s(x)$  as a function of position  $x$ . Parameters are the same as in Fig. 5(a) in the main text, except for that  $\mathbf{m}$  is in the  $y$ - $z$  plane with angles  $45^\circ$  and  $225^\circ$  in the left and right ferromagnetic insulators, respectively.

the spin polarization is perpendicular to the Zeeman field in the ferromagnetic insulator region, and the spin polarization is parallel and along the same direction, in contrast to Fig. 5(a) in the main text, where the Zeeman fields are the same in the left and the right ferromagnetic insulator regions, and the spin polarization is parallel and along the opposite directions. Still, the spin polarization in the superconductor displays a spin helix, and matches well with those in the boundaries. Due to the special condition for the formation of Majorana bound states in the topological insulator systems, a domain wall is needed. So the spin polarization can be well controlled, such as the nonuniform Zeeman fields in the ferromagnetic insulator regions. Therefore the properties of spin polarization are totally different from that in a superconductor-based spin-orbit coupled semiconductor, where the Zeeman field is uniform in the whole system.

- 
- [1] F. Wilczek, *Nat. Phys.* **5**, 614 (2009).  
 [2] S. R. Elliott and M. Franz, *Rev. Mod. Phys.* **87**, 137 (2015).  
 [3] A. Y. Kitaev, *Phys. Usp.* **44**, 131 (2001).  
 [4] D. A. Ivanov, *Phys. Rev. Lett.* **86**, 268 (2001).  
 [5] C. Nayak, S. H. Simon, A. Stern, M. Freedman, and S. Das Sarma, *Rev. Mod. Phys.* **80**, 1083 (2008).  
 [6] A. Y. Kitaev, *Ann. Phys.* **303**, 2 (2003).  
 [7] L. Fu and C. L. Kane, *Phys. Rev. Lett.* **100**, 096407 (2008).  
 [8] L. Fu and C. L. Kane, *Phys. Rev. B* **79**, 161408 (2009).  
 [9] X.-L. Qi, T. L. Hughes, and S.-C. Zhang, *Phys. Rev. B* **82**, 184516 (2010).  
 [10] C. W. J. Beenakker, *Annu. Rev. Condens. Matter Phys.* **4**, 113 (2013).  
 [11] J. D. Sau, R. M. Lutchyn, S. Tewari, and S. Das Sarma, *Phys. Rev. Lett.* **104**, 040502 (2010).  
 [12] J. Alicea, *Phys. Rev. B* **81**, 125318 (2010).  
 [13] R. M. Lutchyn, J. D. Sau, and S. Das Sarma, *Phys. Rev. Lett.* **105**, 077001 (2010).  
 [14] Y. Oreg, G. Refael, and F. von Oppen, *Phys. Rev. Lett.* **105**, 177002 (2010).  
 [15] S. Nadj-Perge, I. K. Drozdov, B. A. Bernevig, and A. Yazdani, *Phys. Rev. B* **88**, 020407 (2013).  
 [16] C. J. Bolech and E. Demler, *Phys. Rev. Lett.* **98**, 237002 (2007).  
 [17] J. Nilsson, A. R. Akhmerov, and C. W. J. Beenakker, *Phys. Rev. Lett.* **101**, 120403 (2008).  
 [18] L. Fu and C. L. Kane, *Phys. Rev. Lett.* **102**, 216403 (2009).  
 [19] A. R. Akhmerov, J. Nilsson, and C. W. J. Beenakker, *Phys. Rev. Lett.* **102**, 216404 (2009).  
 [20] K. T. Law, P. A. Lee, and T. K. Ng, *Phys. Rev. Lett.* **103**, 237001 (2009).  
 [21] K. Flensberg, *Phys. Rev. B* **82**, 180516 (2010).  
 [22] C. Benjamin and J. K. Pachos, *Phys. Rev. B* **81**, 085101 (2010).  
 [23] D. Pikulin, J. Dahlhaus, M. Wimmer, H. Schomerus, and C. Beenakker, *New J. Phys.* **14**, 125011 (2012).  
 [24] E. Prada, P. San-Jose, and R. Aguado, *Phys. Rev. B* **86**, 180503 (2012).  
 [25] E. J. H. Lee, X. Jiang, R. Aguado, G. Katsaros, C. M. Lieber, and S. De Franceschi, *Phys. Rev. Lett.* **109**, 186802 (2012).  
 [26] V. Mourik, K. Zuo, S. Frolov, S. Plissard, E. Bakkers, and L. Kouwenhoven, *Science* **336**, 1003 (2012).  
 [27] M. T. Deng, C. L. Yu, G. Y. Huang, M. Larsson, P. Caroff, and H. Q. Xu, *Nano Lett.* **12**, 6414 (2012).

- [28] J. Liu, A. C. Potter, K. T. Law, and P. A. Lee, *Phys. Rev. Lett.* **109**, 267002 (2012).
- [29] B. H. Wu and J. C. Cao, *Phys. Rev. B* **85**, 085415 (2012).
- [30] F. Crépin, B. Trauzettel, and F. Dolcini, *Phys. Rev. B* **89**, 205115 (2014).
- [31] J. J. He, T. K. Ng, P. A. Lee, and K. T. Law, *Phys. Rev. Lett.* **112**, 037001 (2014).
- [32] A. Haim, E. Berg, F. von Oppen, and Y. Oreg, *Phys. Rev. Lett.* **114**, 166406 (2015).
- [33] H. H. Sun, K. W. Zhang, L. H. Hu, C. Li, G. Y. Wang, H. Y. Ma, Z. A. Xu, C. L. Gao, D. D. Guan, Y. Y. Li, C. Liu, D. Qian, Y. Zhou, L. Fu, S. C. Li, F. C. Zhang, and J. F. Jia, *Phys. Rev. Lett.* **116**, 257003 (2016).
- [34] H. Ebisu, K. Yada, H. Kasai, and Y. Tanaka, *Phys. Rev. B* **91**, 054518 (2015).
- [35] X. Liu, J. D. Sau, and S. Das Sarma, *Phys. Rev. B* **92**, 014513 (2015).
- [36] N. F. Q. Yuan, Y. Lu, J. J. He, and K. T. Law, *Phys. Rev. B* **95**, 195102 (2017).
- [37] K. Bjornson, S. S. Pershoguba, A. V. Balatsky, and A. M. Black-Schaffer, *Phys. Rev. B* **92**, 214501 (2015).
- [38] I. Knez, R. R. Du, and G. Sullivan, *Phys. Rev. Lett.* **109**, 186603 (2012).
- [39] L. P. Gorkov and E. I. Rashba, *Phys. Rev. Lett.* **87**, 037004 (2001).
- [40] F. Crépin, P. Buset, and B. Trauzettel, *Phys. Rev. B* **92**, 100507 (2015).
- [41] D. Sticlet, C. Bena, and P. Simon, *Phys. Rev. Lett.* **108**, 096802 (2012).
- [42] A. Leggett, *Rev. Mod. Phys.* **47**, 331 (1976).
- [43] L. H. Hu, C. Li, D. H. Xu, Y. Zhou, and F. C. Zhang, *Phys. Rev. B* **94**, 224501 (2016).
- [44] S. Das Sarma, J. D. Sau, and T. D. Stanescu, *Phys. Rev. B* **86**, 220506(R) (2012).